AIP | Applied Physics Letters

Yoke-shaped MgO-barrier magnetic tunnel junction sensors

J. Y. Chen, N. Carroll, J. F. Feng, and J. M. D. Coey

Citation: Applied Physics Letters **101**, 262402 (2012); doi: 10.1063/1.4773180
View online: http://dx.doi.org/10.1063/1.4773180
View Table of Contents: http://scitation.aip.org/content/aip/journal/apl/101/26?ver=pdfcov
Published by the AIP Publishing

Yoke-shaped MgO-barrier magnetic tunnel junction sensors

J. Y. Chen,[a] N. Carroll, J. F. Feng,[b] and J. M. D. Coey
School of Physics and CRANN, Trinity College, Dublin 2, Ireland

(Received 5 September 2012; accepted 10 December 2012; published online 26 December 2012)

Yoke-shaped sensors based on MgO-barrier magnetic tunnel junctions have been designed, fabricated, and studied; they show a good linear tunneling magnetoresistance (TMR) response. A nearly-perpendicular configuration of two ferromagnetic electrodes was set by two-step annealing together with shape anisotropy. The low-frequency noise characterization shows these yoke-shaped TMR sensors have relatively low magnetic 1/*f* noise. The field sensitivity is up to 27%/mT, while the field detectivity reaches $4.6\,\mathrm{nT}/\sqrt{\mathrm{Hz}}$ at 10 Hz and $460\,\mathrm{pT}/\sqrt{\mathrm{Hz}}$ at 1 kHz. These TMR sensors may be useful for applications such as biomagnetic detection. © *2012 American Institute of Physics*. [http://dx.doi.org/10.1063/1.4773180]

Magnetoresistive devices have been widely used for magnetic sensing applications, for instance, speed, position, and angle detection in the automotive industry.[1,2] They are also promising candidates for biomagnetic detection such as magnetocardiography (MCG) or for detecting magnetically labeled biomarkers.[3,4] These applications require magnetic sensors with nanotesta or even lower field detectivity in the low frequency range. Magnetic tunnel junctions (MTJs) with a crystalline MgO barrier seem to be a logical choice for such sensor applications due to their large tunnel magnetoresistance (TMR) ratios.[5–7]

However, MTJ devices usually exhibit substantial low-frequency noise with a 1/*f* power spectrum.[8–11] The 1/*f* noise arises either from spin-independent resistance fluctuation within the tunneling barrier due, for example, to charge traps or magnetic fluctuations in the ferromagnetic electrodes due to thermally activated fluctuations of the magnetization. The nonmagnetic 1/*f* noise from the barrier can be substantially reduced by thermal annealing.[12,13] The magnetic 1/*f* noise is the dominant noise source in MTJs. Reducing the magnetic noise is of importance to improve the field detectivity in MTJ (sensor) devices.

Pannetier *et al.*[14] developed a yoke-shaped hybrid giant magnetoresistance (GMR)/superconductor sensor devices with a current-in-plane geometry, which detect magnetic fields in the order of *f*T. The yoke-shaped design provides a stable magnetic domain structure in the long arms of the yoke, which reduces the noise associated with macroscopic domain wall motion.[15,16] However, there are almost no reports of yoke-shaped TMR sensors, because it is hard to obtain the current-perpendicular-to-plane geometry in the MTJ stacks. Here, we report a yoke-shaped TMR sensor device with a MgO barrier. It shows good field sensitivity as well as low detectivity in the low frequency range. By comparing the magnetic noise for different structures, this type of yoke-shaped TMR sensor design seems to be beneficial for low field detection.

Typical MgO-based MTJ stacks with a layer sequence Ta 5/Ru 30/Ta 5/$Ni_{81}Fe_{19}$ (NiFe) 5/$Ir_{22}Mn_{78}$ (IrMn) 10/$Co_{90}Fe_{10}$ 2.5/Ru 0.9/$Co_{40}Fe_{40}B_{20}$ (CoFeB) 3/MgO 2/CoFeB 3/Ta 5/Ru 5 (thicknesses in nanometers) were deposited onto thermally oxidized silicon wafers at room temperature. All metallic multilayers were grown by dc-magnetron sputtering methods, and the MgO layers were grown by rf-sputtering from two MgO targets in a target-facing-target gun in a Shamrock sputtering tool. Yoke-shaped MTJs were patterned by UV lithography and Ar ion milling. High vacuum post-annealing was performed at 350 °C (first anneal) and 100 °C (second anneal) for 1 h in an applied magnetic field of 800 mT. The first annealing step at high temperature sets the exchange bias of the bottom-pinned ferromagnetic layers perpendicular to the long arm of the yoke and induces crystallization of CoFeB at the MgO interfaces, which is necessary for a high TMR ratio. The second anneal at 100 °C with the applied magnetic field parallel to the long arm of the yoke is aimed at resetting the easy axis of the top, free layer.[17] Measurements of magnetoresistance as a function of the direction of the applied field indicate that the angle between the free and pinned layers is about 70°. Both transport and noise were measured by a four-probe method at room temperature. The circuit for the measurement is shown in Fig. 1(a). The low-frequency noise was measured under a constant current bias using a commercial ac coupled low-noise preamplifier (Stanford Research Systems SR552 and SR560). The noise signal was further amplified, filtered, and digitized using a 16-bit National Instruments data acquisition (DAQ) card.

Figure 1(a) shows the schematic design of our yoke-shaped sensors. The long arm of the yoke is around 400 μm, which is designed to fit applications involving a microfluidic channel, used for biomarker detection. Fig. 1(b) shows an optical microscope image of the sensor device with more details of the dimensions. The sensing area is marked by the green oval, which was $4 \times 40\,\mu\mathrm{m}^2$, $4 \times 30\,\mu\mathrm{m}^2$, or $4 \times 20\,\mu\mathrm{m}^2$. Moreover, the junction resistance-area products are of order $10^3 \sim 10^4\,\Omega\,\mu\mathrm{m}^2$ for all TMR sensors used in this work.

Figure 2(a) shows typical TMR curves after the first anneal at 350 °C and after the second anneal at 100 °C for a device with a sensing area of $4 \times 40\,\mu\mathrm{m}^2$. A TMR ratio of 198% was obtained after the first anneal, which indicates high quality of the MgO barrier. After the first anneal at 350 °C, the TMR curve did not exhibit good linearity

[a]chenju@tcd.ie.
[b]Present address: SPINTEC, UMR(8191) CEA/CNRS/UJF/Grenoble INP, INAC, 17 rue des Martyrs, 38054 Grenoble Cedex, France.

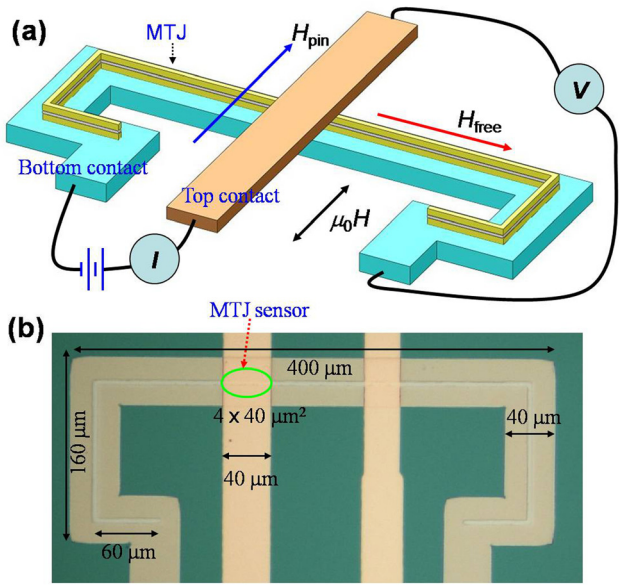

FIG. 1. (a) Three-dimensional schematics of a yoke-shaped TMR sensor design and (b) an optical microscope image shows a real device with two top contacts.

because the orientation of the top, free layer's magnetization set by annealing and shape anisotropy is insufficient to realize the crossed configuration needed for the sensors. The second anneal helps to reset the magnetization of the free layer along the long arm of the yoke. After this step, a good linear TMR response of about 130% was obtained, as shown in the inset of Fig. 2(a). The highest field sensitivity ($s = (1/\mu_0 R)(dR/dH)$) is in the range of 24%–27%/mT. However, the highest field sensitivity is not at zero field due to magnetic coupling between free and pinned ferromagnetic layers. The TMR ratio is diminished after the second anneal because the magnetic orientation of the bottom-pinned IrMn layer has been reset by about 20° to the normal to the yoke.[17] The magnetoresistance can be improved by applying the field at 20° to the normal to the yoke, but the sensor response then becomes hysteretic.

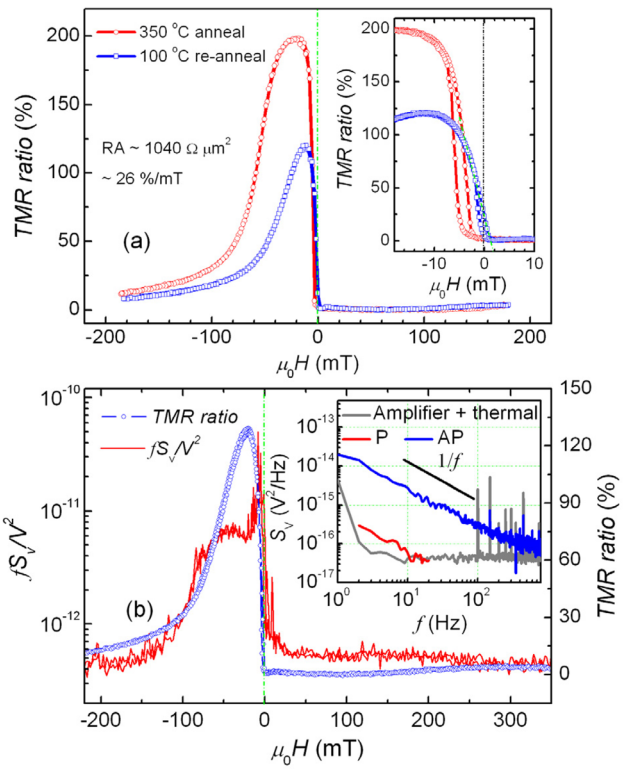

FIG. 2. (a) Typical TMR curves after the first anneal at 350 °C and the second anneal at 100 °C for a yoke-shaped TMR sensor. The inset of (a) shows an enlargement of the transverse TMR curves. (b) The normalized noise and TMR plotted as a function of magnetic field for a yoke-shaped TMR sensor. The inset of (b) shows the 1/*f* noise power spectral density as a function of frequency in the P (80 mT) and AP (−20 mT) states after subtracting the thermal and amplifier noise. Scan rates are ~1.2 mT s^{-1} for (a) and ~0.03 mT s^{-1} for (b).

The inset of Figure 2(b) shows noise power spectral density S_v as a function of f for the two magnetic states in both parallel (P) and antiparallel (AP) configurations of the free and pinned ferromagnetic layers, which are set at 80 mT and −20 mT, respectively. Both states show 1/*f* noise. We parameterize the magnetic 1/*f* noise by a Hooge-like noise parameter $\alpha_{mag} = \Omega f S_{mag}/V^2$, where Ω is the volume of the corresponding ferromagnetic layer, f is the frequency, V is the applied voltage, and S_{mag} is the magnetic power spectral density, determined by subtracting amplifier noise, thermal and shot noise, and the nonmagnetic barrier noise from the measured S_v.[13,18] Figure 2(b) shows the normalized noise parameter and TMR ratio as a function of the applied magnetic field at a bias voltage of 10–30 mV. Both junction resistance and the noise power spectral density centered at 4.8 Hz were measured simultaneously. As shown in Figure 2(b), the magnetic field dependence of the noise parameter fS_v/V^2 exhibits a broad maximum and a sharp peak which are associated with magnetization reversal of two ferromagnetic layers.[17–20] At $\mu_0 H = -5$ mT, the TMR changes rapidly due to the magnetization rotation of the free layer, which means more magnetization fluctuations occur, resulting in more magnetic noise and a sharp noise peak. In the AP state, the magnetizations of free and pinned layers are relatively stable, and the magnetic noise decreases somewhat compared with that of free layer. At $\mu_0 H = -40$ mT, the TMR gradually decreases because of the magnetization reversal of the pinned layer. Slow magnetization fluctuations occur, resulting in less magnetic noise and a very broad maximum.[19] The noise parameter in the P state shows the lowest noise level and is almost independent of magnetic field; it is related to the nonmagnetic barrier resistance noise.[20–22]

In thermal equilibrium, the fluctuation-dissipation theorem can be used to relate the magnetic noise S_{mag} and magnetic susceptibility χ_R. Assuming the imaginary part χ''_R is much smaller than the real part χ'_R, it follows that[13,18]

$$\alpha_{mag} = \frac{\Omega f S_{mag}}{V^2} \approx \varepsilon(H)\frac{k_B T}{\pi M_s}\frac{\Delta R}{R}\left[\frac{1}{\mu_0 R}\frac{dR}{dH}\right], \qquad (1)$$

where $\varepsilon(H) \approx \chi''_R/\chi'_R$ is the phase lag related to magnetic losses in the ferromagnetic layers, ΔR is the total resistance change between the P and AP states. Equation (1) shows that the magnetic noise parameter α_{mag} is proportional to the field sensitivity if ε is independent of field. α_{mag} for both free and pinned layers of different structures as a function of field sensitivity is shown in Fig. 3. A roughly linear scaling is observed for both pinned and free layers of all the MTJ

structures. The linear dependence on field sensitivity means that the phase lag ε is a constant and independent of field. The linear dependence has been previously reported in AlO_x and MgO MTJs.[9,10,19,23–25] With their lower field sensitivity values ($\leq 1\%/\text{mT}$), the yoke-shaped GMR sensor shows the lowest magnetic noise level. But from the applications point of view, low field sensitivity is not what is needed for a sensor. Because the highest GMR ratio is around 10%,[14] based on Eq. (1), the phase lag of the free layer for a GMR structure becomes comparable to or lower than that for a yoke-shaped TMR sensor. For the MTJ stacks, the magnetic noise for double-pinned stacks is at the same level as the normal bottom-pinned MTJ stacks.[17] However, the yoke-shaped TMR sensors show a magnetic noise up to one order lower than the other devices. Moreover, they have the highest field sensitivity, especially for the free layer. This is evidence that the yoke has a stable magnetic configuration resulting in a low phase lag.

The sensor's equivalent field noise in units of T^2/Hz can be determined from[17,18]

$$S_B = \frac{\alpha_{mag}}{f\Omega_{free}}\left[\frac{1}{\mu_0 R}\frac{dR}{dH}\right]^{-2}. \quad (2)$$

Using data from Figure 3 for the free layer, the field detectivity $\sqrt{S_B}$ of our yoke-shaped TMR sensors is about $14.5\,\text{nT}/\sqrt{\text{Hz}}$ at 1 Hz, which is better than many other types of TMR sensors,[10,17,26,27] and it decreases further with frequency. Figure 4(a) presents the frequency dependence of field detectivity for a yoke-shaped TMR sensor and the double-pinned TMR pillar sensor.[17] It shows the field detectivity of yoke-shaped TMR sensor is better than $1\,\text{nT}/\sqrt{\text{Hz}}$ at 1 kHz, which is 2–3 times lower than GMR sensors[18] and better than double-pinned TMR sensor.[17] It could be further

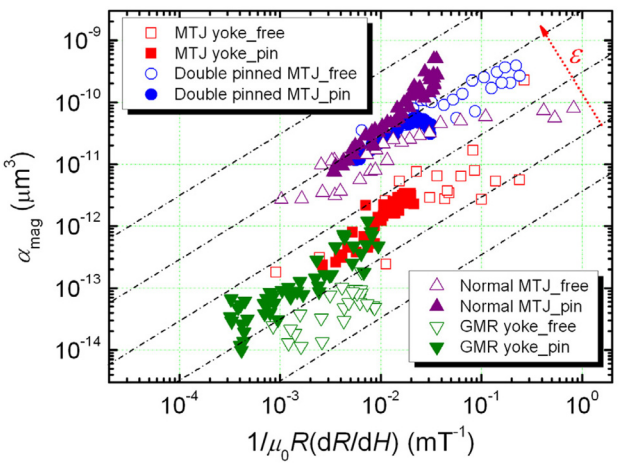

FIG. 3. Magnetic noise parameter plotted as a function of field sensitivity for different magnetic structures. All data shown are for free (open symbols) and pinned layers (solid symbols) in our normal bottom-pinned MgO MTJs annealed at 350 °C (the MTJ stacks are the same as the yoke-shaped MTJ sensors) (△, ▲), double-pinned MgO MTJs (The stack: Ta 5/Ru 30/Ta 5/NiFe 5/IrMn 10/CoFe 2.5/Ru 0.9/CoFeB 3/MgO 2/CoFeB 3/Ru 0.3/IrMn 6/NiFe 5/Ta 5/Ru 5 (units in nm)) are annealed by two steps with the first step at 350 °C and the second step at 150 °C) (◦, •), yoke-shaped MTJs (□, ■), and yoke-shaped GMR spin valves in the as-grown state (The stack: Ta 5/NiFe 3/CoFe 5/Cu 2.8/CoFe 5/IrMn 10/Ta 5 (units in nm)) (▽, ▼). The dashed lines with slope 1 are guides to the eye.

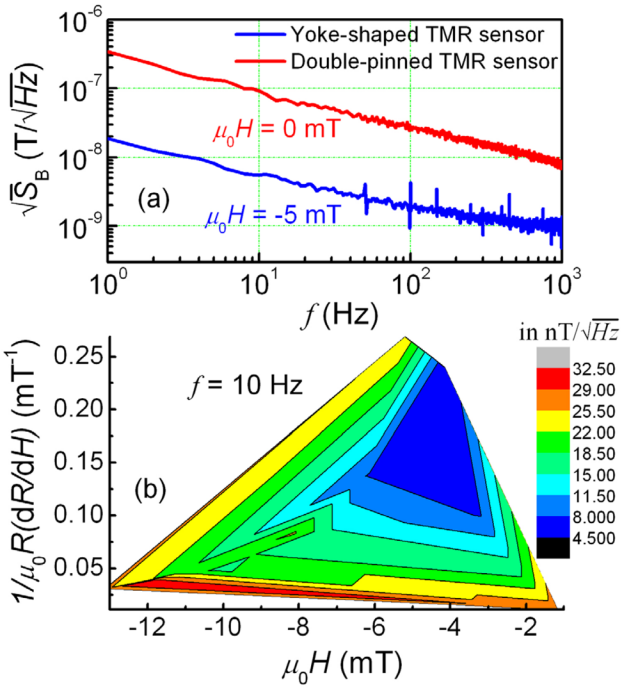

FIG. 4. (a) Typical field detectivity as a function of frequency for a yoke-shaped TMR sensor and a double-pinned TMR sensor (the device is a circular pillar with diameter of 4 μm); (b) The typical field detectivity map of a yoke-shaped TMR sensor (in units $\text{nT}/\sqrt{\text{Hz}}$) plotted as a function of field sensitivity and magnetic field.

improved by using a flux concentrator.[28] Better values of field detectivity have only obtained in this way.[29–32] For example, Chaves *et al.* have reported a value of field detectivity of $51\,\text{pT}/\sqrt{\text{Hz}}$ at 30 Hz and field sensitivity of 870%/mT by using a flux concentrator.[29,30] The relation of magnetic field, field sensitivity, and field detectivity is plotted in Figure 4(b). The lowest field detectivity appears when field is in the range of −4 mT to −5 mT, while the highest field sensitivity occurs at −6 mT. In other words, the highest field sensitivity does not match the lowest field detectivity. The reason is that magnetic noise is normally highest when the field sensitivity is highest. Similar results were reported in Ref. 33.

In conclusion, yoke-shaped TMR sensors based on MgO-barrier MTJs have been built and evaluated. Their field sensitivity is in the range of 24%–27%/mT, and the field detectivity reaches $460\,\text{pT}/\sqrt{\text{Hz}}$ at 1 kHz. They have lower magnetic noise compared with other types of TMR sensors due to the stable magnetic configuration of the yoke, and have better field detectivity than for yoke-type GMR sensors. The overall improvement in field detectivity of the yoke-shaped TMR sensor devices may be decisive for their applications.

The authors thank Bo Cui from University of Waterloo, Canada, K. Oguz, H. Kurt, and D. Ménard for helpful discussions. The work was supported by the EU as part of FP7 NAMDIATREAM Project and by Science Foundation Ireland as part of the Nanoscale Interface and Spin Electronics (NISE) Project (10/IN1/I3006).

[1]C. Tsang, R. E. Fontana, T. Lin, D. E. Heim, V. S. Speriosu, B. A. Gurney, and M. L. Williams, IEEE Trans. Magn. **30**, 3801 (1994).

[2]G. Rieger, K. Ludwig, J. Hauch, and W. Clemens, Sens. Actuators, A **91**, 7 (2001).
[3]M. Pannetier-Lecoeur, L. Parkkonen, N. Sergeeva-Chollet, H. Polovy, C. Fermon, and C. Fowley, Appl. Phys. Lett. **98**, 153705 (2011).
[4]P. P. Freitas, F. A. Cardoso, V. C. Martins, S. A. M. Martins, J. Loureiro, J. Amaral, R. C. Chaves, S. Cardoso, L. P. Fonseca, A. M. Sebastião, M. Pannetier-Lecoeur, and C. Fermon, Lab Chip **12**, 546 (2012).
[5]S. S. P. Parkin, C. Kaiser, A. Panchula, P. M. Rice, B. Hughes, M. Samant, and S. H. Yang, Nature Mater. **3**, 862 (2004).
[6]S. Yuasa, A. Fukushima, T. Nagahama, K. Ando, and Y. Suzuki, Nature Mater. **3**, 868 (2004).
[7]S. Ikeda, J. Hayakawa, Y. Ashizawa, Y. M. Lee, K. Miura, H. Hasegawa, M. Tsunoda, F. Matsukura, and H. Ohno, Appl. Phys. Lett. **93**, 082508 (2008).
[8]E. R. Nowak, M. B. Weissman, and S. S. P. Parkin, Appl. Phys. Lett. **74**, 600 (1999).
[9]L. Jiang, E. R. Nowak, P. E. Scott, J. Johnson, J. M. Slaugher, J. J. Sun, and R. W. Dave, Phys. Rev. B **69**, 054407 (2004).
[10]C. Ren, X. Y. Liu, B. D. Schrag, and G. Xiao, Phys. Rev. B **69**, 104405 (2004).
[11]J. Scola, H. Polovy, C. Fermon, M. Pannetier-Lecoeur, G. Feng, K. Fahy, and J. M. D. Coey, Appl. Phys. Lett. **90**, 252501 (2007).
[12]S. H. Liou, R. Zhang, S. E. Russek, L. Yuan, S. T. Halloran, and D. P. Pappas, J. Appl. Phys. **103**, 07E920 (2008).
[13]R. Stearrett, W. G. Wang, L. R. Shah, J. Q. Xiao, and E. R. Nowak, Appl. Phys. Lett. **97**, 243502 (2010).
[14]M. Pannetier, C. Fermon, G. Le Goff, J. Simola, and E. Kerr, Science **304**, 1648 (2004).
[15]M. Pannetier, C. Fermon, G. Le Goff, J. Simola, E. Kerr, and J. M. D. Coey, J. Magn. Magn. Mater. **290**, 1158 (2005).
[16]Z. Diao, E. R. Nowak, K. M. Haughey, and J. M. D. Coey, Phys. Rev. B **84**, 094412 (2011).
[17]J. Y. Chen, J. F. Feng, and J. M. D. Coey, Appl. Phys. Lett. **100**, 142407 (2012).
[18]A. Ozbay, A. Gokce, T. Flanagan, R. A. Stearrett, E. R. Nowak, and C. Nordman, Appl. Phys. Lett. **94**, 202506 (2009).
[19]R. Stearrett, W. G. Wang, X. M. Kou, J. F. Feng, J. M. D. Coey, J. Q. Xiao, and E. R. Nowak, Phys. Rev. B **86**, 014415 (2012).
[20]G. Q. Yu, Z. Diao, J. F. Feng, H. Kurt, X. F. Han, and J. M. D. Coey, Appl. Phys. Lett. **98**, 112504 (2011).
[21]R. Stearrett, W. G. Wang, L. R. Shah, A. Gokce, J. Q. Xiao, and E. R. Nowak, J. Appl. Phys. **107**, 064502 (2010).
[22]Z. Diao, J. F. Feng, H. Kurt, G. Feng, and J. M. D. Coey, Appl. Phys. Lett. **96**, 202506 (2010).
[23]J. F. Feng, Z. Diao, G. Feng, E. R. Nowak, and J. M. D. Coey, Appl. Phys. Lett. **96**, 052504 (2010).
[24]S. Ingvarsson, G. Xiao, S. S. P. Parkin, W. J. Gallagher, G. Grinstein, and R. H. Koch, Phys. Rev. Lett. **85**, 3289 (2000).
[25]J. F. Feng, Z. Diao, H. Kurt, R. Stearrett, A. Singh, E. R. Nowak, and J. M. D. Coey, J. Appl. Phys. **112**, 093913 (2012).
[26]J. M. Almeida, P. Wisniowski, and P. P. Freitas, J. Appl. Phys. **103**, 07E922 (2008).
[27]D. Mazumdar, X. Y. Liu, B. D. Schrag, W. F. Shen, M. Carter, and G. Xiao, J. Appl. Phys. **101**, 09B502 (2007).
[28]A. Jander, C. A. Nordman, A. V. Pohm, and J. M. Anderson, J. Appl. Phys. **93**, 8382 (2003).
[29]R. C. Chaves, P. P. Freitas, B. Ocker, and W. Maass, Appl. Phys. Lett. **91**, 102504 (2007).
[30]R. C. Chaves, P. P. Freitas, B. Ocker, and W. Maass, J. Appl. Phys. **103**, 07E931 (2008).
[31]S. H. Liou, D. Sellmyer, S. E. Russek, R. Heindl, F. C. S. Da Silva, J. Moreland, D. P. Pappas, L. Yuan, and J. Shen, Proceedings of the 8th Annual IEEE Conference on Sensors, 1848–1851 (2009).
[32]S. H. Liou, X. L. Yin, S. E. Russek, R. Heindl, F. C. S. Da Silva, J. Moreland, D. P. Pappas, L. Yuan, and J. Shen, IEEE Trans. Magn. **47**, 3740 (2011).
[33]D. Mazumdar, W. F. Shen, X. Y. Liu, B. D. Schrag, M. Carter, and G. Xiao, J. Appl. Phys. **103**, 113911 (2008).